Corrosion Benefits of Piperazine As an Alternative CO 2 Capture Solvent

ARTICLE *in* INDUSTRIAL & ENGINEERING CHEMISTRY RESEARCH · JULY 2014

Impact Factor: 2.59 · DOI: 10.1021/ie501346z

4 AUTHORS, INCLUDING:

Liangfu Zheng
University of Kentucky
13 PUBLICATIONS **9** CITATIONS
SEE PROFILE

James Landon
University of Kentucky
28 PUBLICATIONS **213** CITATIONS
SEE PROFILE

I&EC research
Industrial & Engineering Chemistry Research

Article

pubs.acs.org/IECR

Corrosion Benefits of Piperazine As an Alternative CO_2 Capture Solvent

Liangfu Zheng, James Landon, Wenchen Zou, and Kunlei Liu*

Center for Applied Energy Research, University of Kentucky, 2540 Research Park Drive, Lexington, Kentucky 40511-8410, United States

Supporting Information

ABSTRACT: The corrosion behavior of A106 carbon steel in piperazine, an advanced alternative postcombustion CO_2 capture solvent to monoethanolamine, has been investigated. Electrochemical corrosion testing methods such as linear polarization resistance (LPR) and electrochemical impedance spectroscopy (EIS) have been used to evaluate the corrosion of A106 in 0.43 mol CO_2/mol alkalinity (C/N) loaded 30 wt % piperazine at 80 °C for 150 h. In addition, immersion corrosion has been carried out up to 1050 h in a traditional corrosion cell with the same CO_2 loaded solution but at 100 °C and 110 psi. Subsequently, as-corroded A106 samples were characterized by scanning electron microscopy/energy dispersive spectroscopy (SEM/EDS) and X-ray diffraction (XRD). The results showed that a sharp decrease in the corrosion rate occurred before reaching a steady-state corrosion process. This was due to the growth of a protective and stable layer of $FeCO_3$. Possible mechanisms are discussed.

1. INTRODUCTION

Anthropogenic carbon dioxide generation from the combustion of fossil fuels such as coal and natural gas has been discussed considerably in recent years as a contributor to climate change. One effective mitigation option is to adopt postcombustion CO_2 capture and sequestration, which is a process consisting of the separation of CO_2 from industrial and energy-related sources by typically using aqueous solutions of alkanolamines such as monoethanolamine (MEA), and then transporting pressurized CO_2 to a storage location for long-term isolation from the atmosphere.[1−3] One of the issues for the application of this process is corrosion. The documented results have shown that CO_2 loaded aqueous solutions of alkanolamines are highly corrosive not only to carbon steels with little alloying of chromium but also to stainless steels with chromium content up to approximately 20 wt %, which is exacerbated in the presence of oxygen and H_2S.[4−17] This can directly affect the whole system efficiency as well as the economics due to solvent losses, unplanned downtime, reduced equipment lifetime, and even health and safety issues. To decrease corrosion in current commercial CO_2 capture systems without affecting its CO_2 capture efficiency and significantly increasing cost, several methods can be adopted such as the use of corrosion inhibitors, application of alternative solvents with low corrosivity, as well as the design of protective coatings.[3,4,11,18−25] Among these methods, much attention has been given lately to looking for new alternative solvents.[3,4,18−25]

Recent studies have shown that piperazine (PZ), a cyclic secondary amine with two nitrogen groups, has some attractive advantages such as a low thermal degradation rate up to 150 °C, a low oxidation rate in the presence of ions of Cr, Ni, Fe, and V or their combinations, low regeneration energy, and a fast CO_2 absorption rate.[19−21] This makes PZ an attractive alternative solvent even with some disadvantages such as high viscosity and a narrow solubility window in lean CO_2 capture solutions, which could preclude its use as a single operational process solvent. Moreover, PZ has been routinely reported to be an effective promoter of the absorption rate in CO_2 capture solutions.[22−25] Corrosion of steels in some of these blends has been conducted recently.[25] However, knowledge of the corrosion behavior of materials in a concentrated PZ solution is still lacking. Investigation of the corrosion of materials (especially steels) in PZ is not only necessary to understand the mechanism of the corrosion of materials in the existing blends with PZ, such as promoted methyldiethanolamine (MDEA), but also to develop new PZ activated blends as well as to apply PZ as a single solvent for CO_2 capture in the future.

Furthermore, to the best of our knowledge, most of the reported papers have been conducted using short-term electrochemical testing while long-term immersion corrosion testing of steels in postcombustion CO_2 capture systems at conditions relevant to the stripper and absorber columns, the reboilers, heat exchangers, and pipes has been lacking.[5−17,25] In this work, in addition to electrochemical testing, an investigation of the corrosion of carbon steel has been conducted by long-term immersion testing for a continuous time period of 1050 h using a CO_2 loaded concentrated PZ solution, normally greater than 30 wt %, with which absorption-stripping is an advanced solvent for postcombustion CO_2 capture from coal-fired power plants.[19−21] Carbon loaded PZ will be shown to result in a substantially lower corrosion rate for carbon steel than comparable amine capture solutions.

2. EXPERIMENTAL SECTION

Normally, the highest corrosion occurs in the carbon-rich section of a CO_2 capture unit that is operated under high temperature and pressure as well as fast movement of solutions.

Received: March 31, 2014
Revised: June 4, 2014
Accepted: June 30, 2014
Published: June 30, 2014

dx.doi.org/10.1021/ie501346z | Ind. Eng. Chem. Res. 2014, 53, 11740−11746

Table 1. Nominal Chemical Composition of A106 Grade B Carbon Steel (wt %)

C	Si	Mn	P	S	Cr	Mo	Ni	Cu	V	Al	Fe
0.27	0.26	0.86	0.013	0.022	0.12	0.04	0.15	0.21	0.001	0.044	bal

Therefore, to simulate higher corrosion in a postcombustion CO_2 capture system, A106 grade B carbon steel, usually designed to be used as seamless pipe in high temperature and pressure applications, was chosen to perform corrosion testing in 30 wt % PZ with the balance being deionized water. The nominal chemical compositions of A106 are listed in Table 1. Samples, including cylinders with dimensions of Φ 9.5 mm × 13 mm and coupons with dimensions of 40 mm × 13 mm × 2 mm, were cut from A106 pipes. The cylinders were used for electrochemical testing under static conditions, and the coupons were used for long-term immersion testing under a circulated system. All of the samples were ground with SiC sand paper from 240, 400, 600, to 800# and then ultrasonically cleaned with deionized water and acetone.

2.1. Short-Term Electrochemical Testing. The effect of exposure duration on the corrosion of A106 in 30 wt % PZ with a CO_2 loading of 0.43 mol CO_2/mol alkalinity (C/N), a total alkalinity of 6.14 mol/kg, a bulk pH of 8.97, and a density of 1.13 g/mL at 80 °C was examined by electrochemical measurements. An electrochemical corrosion unit with a standard three-electrode setup was used for electrochemical testing with a saturated calomel electrode (SCE) as the reference electrode, and a graphite rod as the counter electrode, as can be seen in our previous work.[10] Electrochemical experiments were performed by a Reference 600 Potentiostat/Galvanostat/ZRA (Gamry Instrument, Warminster, PA, USA). Linear polarization resistance (LPR) testing was conducted at 1 h after reducing potentiostatically at −1.2 V (vs SCE) for 120 s. For LPR testing, the samples were polarized from −10 to 10 mV vs open circuit voltage (E_{corr}) with a scan rate of 0.166 mV/s. In addition, electrochemical impedance spectroscopy (EIS) testing was performed after LPR testing. EIS measurements were performed using an AC signal at the E_{corr} with a perturbation amplitude of 10 mV RMS (root-mean-square) and a frequency range from 100 kHz to 0.01 Hz. All the impedance plots shown in this paper have been normalized to the original geometric surface area of the samples. Because the laboratory electrochemical testing cell can only be operated at ambient pressure, more extreme corrosion conditions with high pressure and higher temperature were examined in a traditional corrosion cell for long-term investigations.

2.2. Long-Term Immersion Corrosion. A traditional corrosion cell, which can be used at elevated temperature and pressure more relevant to the conditions present in the stripper column of a CO_2 capture process in a power plant, was used for long-term immersion corrosion testing. The details of the traditional corrosion cell have been described in our previous work.[10] The tested solution was the same as for electrochemical testing, i.e., 30 wt % PZ with a total CO_2 loading of 0.43 C/N. After measurements of the dimensions and weight, the coupons were hung onto racks and separated by teflon spacers with a length of 10 mm. Thereafter, the racks with coupons were put into the traditional corrosion cell and fully submerged into prepared volumes of solution (approximately 4 L) according to ASTM G4-95.[26] To minimize the effect of O_2 on the corrosion rate for this experiment, the system was purged with CO_2 with a flow rate of 4 L/min for 1 h to remove residual air in the head zone of pressure vessel before every run. The solution was circulated by a pump between a heat exchanger cell and the traditional corrosion cell where the coupons are placed. The testing temperature was 100 °C, and the pressure was 110 psi. A continuous corrosion investigation over 1050 h has been performed. A set of samples was removed every 150 h to study the impact of duration on the corrosion. The remaining sets of samples were carefully returned to the traditional cell for further corrosion testing.

After being removed, the coupons were cleaned. To prevent destruction of the corrosion product from the sample surface by force, the samples were submerged carefully in DI water and acetone sequentially, and then placed in individually labeled plastic sealed sample bags after being slowly dried by compressed air. Samples were stored in a vacuum desiccator until further analysis was conducted. Storage under vacuum was used to prevent further oxidation of the corroded samples before characterization.

Before sealing the traditional cell for the next 150 h run, reconditioning of the solution was conducted to compensate for the loss of solvent and carbon dioxide captured, i.e. the parameters of carbon loading and alkalinity were reconditioned to approximately the original set points. The aim of reconditioning was to reestablish similar operating conditions for the duration of each run.

To calculate the corrosion rate of A106 by the weight loss method, coupons were selected after corrosion of varying durations and were chemically cleaned for removal of the corrosion product according to ASTM G1-90 with a liter of solution containing 500 mL of hydrochloric acid (HCl, sp gr 1.19), 3.5 g of hexamethylene tetramine, and reagent water at room temperature for 35 min.[27] Thereafter, the coupons were cleaned, dried, and weighed quickly. The corrosion rate (R, mmpy) was calculated using the following equation (eq 1):

$$R = \frac{8.76 \times 10^6 (m_0 - m_1)}{St\rho} \quad (1)$$

where m_0, m_1, S, t, and ρ are the weight before corrosion (g), weight after removal of corrosion product (g), sample surface area (mm^2), immersion duration (h), and density of the tested material (g/cm^3), respectively.

2.3. Characterization Methods. To understand the corrosion mechanisms for A106 in CO_2-loaded PZ under different durations, the collected coupons were characterized using scanning electron microscopy/energy dispersive spectroscopy (SEM/EDS) and X-ray diffraction (XRD). A Hitachi S-4800 field emission SEM/EDS was used to characterize surface morphologies of the corroded samples and to analyze the corresponding elemental composition of the as-formed corrosion product. After XRD and SEM/EDS characterization, select samples were sealed using a nondestructive resin and subsequently ground and polished for cross-sectional characterization. A voltage of 15 kV and a current of 20 μA were used for SEM/EDS characterizations. All XRD scans were carried out using the Rigaku Smartlab 1 kW powder system equipped with a Cu target. The operation voltage and current were 40 kV and 44 mA, respectively. The size of the beam-defining collimating slit was 5 × 10 mm. For the samples from electrochemical cell, a 2-θ mode was used with a low grazing angle of X-ray

dx.doi.org/10.1021/ie501346z | Ind. Eng. Chem. Res. 2014, 53, 11740−11746

incidence (omega) of 1°, and the 2-θ range of the detector from 15 to 115°. For samples from the traditional corrosion cell, a θ/2-θ mode was used with 2-θ ranges from 15 to 115°.

2.4. Solution Analysis. The alkalinity of the solutions was determined by acid titration using a MetrohmTitrando 836. The CO_2 content of the loaded solutions were analyzed by an acid−base method. In this method, phosphoric acid liberates CO_2 from MEA solutions, which is carried out by nitrogen gas before being fed into a HORIBA CO_2 analyzer (VIA-510) for quantitative determination. The pH was measured at ambient temperature using a temperature corrected probe and 2 point calibration. The density was measured by dispensing 1000 μL of solution in quadruplicate and determining mass.

3. RESULTS AND DISCUSSION

3.1. Short-Term Corrosion Testing. *3.1.1. LPR Testing.* Figure 1 shows the corrosion rate of A106 in 30 wt % PZ with a

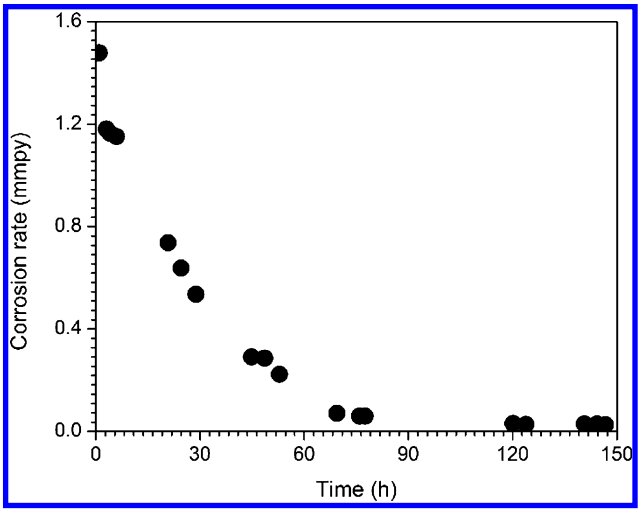

Figure 1. Corrosion rates of A106 carbon steel in 0.43 C/N CO_2 loaded 30 wt % PZ at 80 °C, obtained by LPR testing, as a function of exposure duration.

CO_2 loading of 0.43 C/N at 80 °C as a function of exposure time. As can be seen, the corrosion rate decreased sharply from approximately 1.48 mmpy after 1 h to approximately 0.06 mmpy after 78 h. Thereafter, a steady-state corrosion process with a corrosion rate of 0.03 mmpy was observed with increases in duration up to 150 h. The corrosion rate is about 2 orders of magnitude lower than that in 0.43 C/N CO_2 loaded 30 wt % MEA under the same testing conditions (see Supporting Information). To understand the corrosion behavior in PZ, SEM/EDS and XRD have been used to characterize the as-corroded samples for various immersion durations.

3.1.2. Characterization for As-Corroded Samples. Figure 2 shows the SEM surface and cross-sectional morphologies after immersion for 1 (just before LPR testing), 4, 14.5, and 147 h (the end of testing). From Figure 2a, most of the surface of the A106 carbon steel was covered by a thin layer of corrosion product with cubically shaped clusters after the first hour. This is completely different from the corrosion of carbon steels in similar solutions of 50 wt % MDEA with a carbon loading of 0.13 C/N and 30 wt % MEA with a carbon loading of 0.43 C/N, in which no notable layer of corrosion product were found to be formed on the metal surface even after several days except for porous residual Fe_3C with a lamellar structure on its

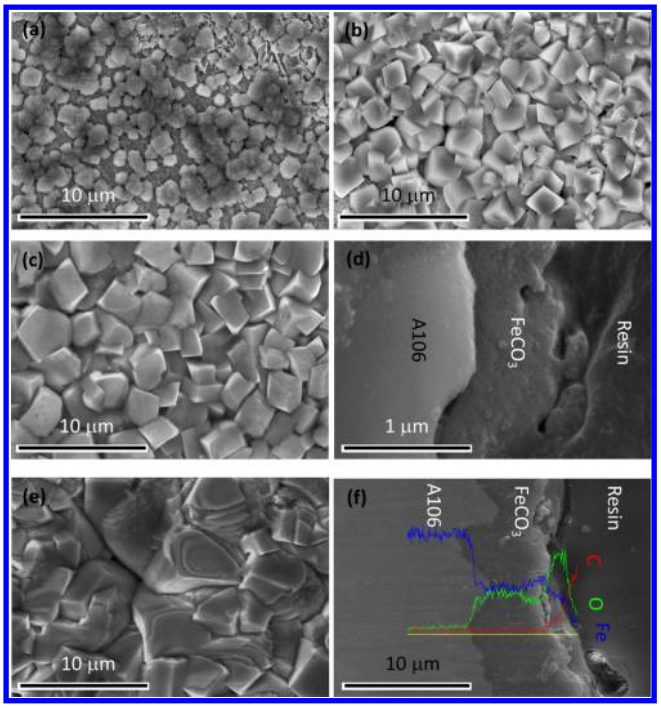

Figure 2. SEM surface morphologies of A106 carbon steel after exposure in 0.43 C/N CO_2 loaded 30 wt % PZ solution at 80 °C for (a) 1, (b) 4, (c) 14.5, and (e) 147 h. (d) and (f) Cross-sectional images corresponding to parts (c) and (e), respectively.

surface.[28] (and see Supporting Information) This difference may be due to slow kinetics for its formation as a corrosion product in the localized conditions at the surface of carbon steels in these solutions. Under these circumstances, the dissolving rate of carbon steel would be always high.[28] (and see Supporting Information) On the contrary, once a layer of corrosion product was formed on the surface of A106, it can inhibit the corrosion process by presenting a diffusion barrier for the species involved in the corrosion process from migrating into the bulk solvent.

Coverage of the surface by corrosion product increased with increases in time (Figure 2a, b, and c), and the surface was found to be covered completely after 14.5 h with a layer of corrosion product, as shown in Figure 2c. Its corresponding grazing incidence XRD patterns show the formed corrosion product is $FeCO_3$ (see Figure 3a). An approximately 1 μm-thick layer of the as-formed $FeCO_3$ was observed on most of the surface areas after 14.5 h, as can be seen from its corresponding cross-sectional morphology given in Figure 2d. Both the size of the clusters and the thickness of the as-formed $FeCO_3$ layer increased with increases in exposure time to 147 h, as shown in Figure 2e for its surface morphology and Figure 2f for its cross-sectional morphology and corresponding elemental linear scanning result. The interface between A106 and $FeCO_3$ is uneven, which might be partly due to the samples preparation and partly due to the selective dissolution of the ferrite phase relative to the pearlite phase in A106, i.e., the galvanic corrosion occurring at the beginning.[28,29] Also, thickening of the layer with an increase in exposure time was observed to result in weakening/disappearance of the diffraction peaks for A106 carbon steel as shown for 14.5 h in Figure 3a and 147 h in Figure 3b. In addition, the as-formed $FeCO_3$ was dense (Figure 2e and f). Whether the layer is dense or not depends primarily on the growth of the $FeCO_3$ layer, i.e.,

dx.doi.org/10.1021/ie501346z | Ind. Eng. Chem. Res. 2014, 53, 11740−11746

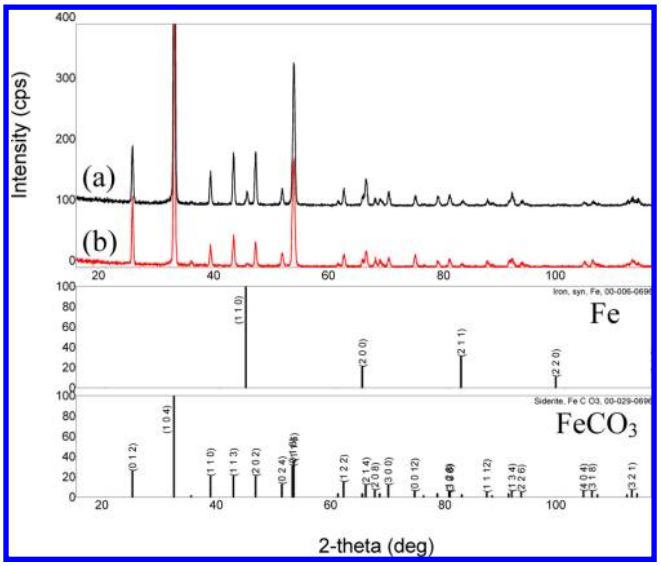

Figure 3. Grazing incidence XRD patterns for A106 after corrosion in 0.43 C/N CO_2 loaded 30 wt % PZ solution at 80 °C for (a) 14.5 and (b) 147 h to show the formation of $FeCO_3$.

the precipitation/growth rate among other factors. As more $FeCO_3$ precipitates/grows, the film grows in density as well as thickness (see Figure 2). However, dissolution of A106 can occur under the as-formed layer, which would result in the continuous creation of "voids" between the layer and the A106 surface. As soon as these voids are created, the voids start to be filled up by the ongoing precipitation/growth. When the rate of precipitation/growth at the A106 surface equals or exceeds the rate of dissolution, a dense protective film forms.[30] That is, the dissolution of A106 is the rate-determining step for growth of the $FeCO_3$ layer. This resulted in little or no cavities or cracks on the as-formed $FeCO_3$ and/or at the interface between $FeCO_3$ and the A106 substrate, as shown in its corresponding cross-sectional image in Figure 2f. This indicates that the as-formed $FeCO_3$ is not just dense as observed from its surface morphology (Figure 2e) but cohesive to the A106 substrate. Alternatively, when the dissolution process occurs under the newly formed film faster than precipitation/growth can fill in the voids, a porous and nonprotective film forms, which can be sometimes very thick but still nonprotective, as occurs under certain conditions in CO_2-loaded MEA solutions.[7,30] Therefore, the sharp decrease in the corrosion rate for A106 before 78 h (see Figure 1) is due to the increase in coverage by the formed $FeCO_3$ layer, i.e., decreased pathways for corrosive species to reach the surface of A106 with the growth of an $FeCO_3$ layer. When the $FeCO_3$ coverage reached a critical value, the corrosion rate continued at a substantially lower value than the initial corrosion rate.

To fully understand the formation of the layer of $FeCO_3$ under these conditions, thermodynamic calculations were conducted as per the procedure shown in ref 31. From the reported results, the iron species including magnetite (Fe_3O_4), hematite (Fe_2O_3), and $FeCO_3$ are the most prevalent corrosion product formed in CO_2-containing solutions.[8,31] Therefore, the following reactions between Fe and $FeCO_3$ (eq 2), Fe_3O_4 and $FeCO_3$ (eq 3), and Fe_2O_3 and $FeCO_3$ (eq 4), i.e., the boundaries for the region to form $FeCO_3$ in a Pourbaix diagram, were considered.[8,31] The corresponding Nernst equations to eqs 2−4 are given in eqs 5−7, respectively.

$$FeCO_3 + 2H^+ + 2e^- \leftrightarrow Fe + H_2O + CO_2 \quad (2)$$

$$Fe_3O_4 + 3CO_2 + 2H^+ + 2e^- \leftrightarrow 3FeCO_3 + H_2O \quad (3)$$

$$Fe_2O_3 + 2CO_2 + 2H^+ + 2e^- \leftrightarrow 2FeCO_3 + H_2O \quad (4)$$

$$E_{r(FeCO_3/Fe)} = E^\circ_{r(FeCO_3/Fe)} + \frac{RT}{2F}\ln\left(\frac{{c_{H^+}}^2}{P_{CO_2}}\right) \quad (5)$$

$$E_{r(Fe_3O_4/FeCO_3)} = E^\circ_{r(Fe_3O_4/FeCO_3)} + \frac{RT}{2F}\ln({c_{H^+}}^2 {P_{CO_2}}^3) \quad (6)$$

$$E_{r(Fe_2O_3/FeCO_3)} = E^\circ_{r(Fe_2O_3/FeCO_3)} + \frac{RT}{2F}\ln({c_{H^+}}^2 {P_{CO_2}}^2) \quad (7)$$

$$\ln P_{(CO_2)}\,(\mathrm{Pa}) = 35.5 - \frac{11065}{T} - 22.4a^2 + 4702\frac{a}{T} + 11699\frac{a^2}{T} \quad (8)$$

where $E_{r(FeCO_3/Fe)}$, $E_{r(Fe_3O_4/FeCO_3)}$, and $E_{r(Fe_2O_3/FeCO_3)}$ are the reversible potentials for reactions of eqs 2−4, respectively. Correspondingly, $E^\circ_{r(FeCO_3/Fe)}$, $E^\circ_{r(Fe_3O_4/FeCO_3)}$, and $E^\circ_{r(Fe_2O_3/FeCO_3)}$ are the reversible potentials at standard conditions using unit concentrations and reference temperature and pressure. R, T, F, c_{H^+}, and P_{CO_2} are the gas constant, the temperature, Faraday's constant, the concentration of H^+, and the partial pressure of CO_2, respectively. P_{CO_2} can be calculated from a reported empirical model for CO_2-loaded PZ as given in eq 8.[32] After substitution of all of the data into the equations, the simplified Nernst equations of eqs 5−7 were obtained and listed as in eqs 9−11, respectively.

$$E_{rev(FeCO_3/Fe)} = -0.377 - 0.070\mathrm{pH} \quad (9)$$

$$E_{rev(Fe_3O_4/FeCO_3)} = 0.692 - 0.070\mathrm{pH} \quad (10)$$

$$E_{rev(Fe_2O_3/FeCO_3)} = 0.509 - 0.070\mathrm{pH} \quad (11)$$

For a solution of 0.43 C/N loaded 30 wt % PZ, the bulk pH value was 8.97. Therefore, an approximate potential range in which $FeCO_3$ can be formed as the corrosion product was found to be between −1.005 and −0.119 V vs SHE. The corrosion potential is approximately −0.800 V vs SCE at 80 °C, i.e. approximately −0.559 V vs SHE, which is in the potential range to form $FeCO_3$.

Therefore, similar to corrosion of carbon steel in CO_2 loaded MEA, the corrosion behavior of A106 enhanced by CO_2 loaded PZ can possibly be explained by the reactions listed as follows (eqs 12−22).[8,14,19,33,34]

Absorption of CO_2 into PZ:

$$2PZ + CO_2 \leftrightarrow PZH^+ + PZCOO^- \quad (12)$$

$$CO_2 + PZ + H_2O \leftrightarrow PZH^+ + HCO_3^- \quad (13)$$

$$CO_2 + PZH^+ + H_2O \leftrightarrow H^+PZCOO^- + H_3^+O \quad (14)$$

$$PZCOO^- + CO_2 + H_2O \leftrightarrow H^+PZCOO^- + HCO_3^- \quad (15)$$

$$2H_2O + CO_2 \leftrightarrow H_3O^+ + HCO_3^- \quad (16)$$

Dissociation of the bicarbonate ion:

dx.doi.org/10.1021/ie501346z | Ind. Eng. Chem. Res. 2014, 53, 11740−11746

$$H_2O + HCO_3^- \leftrightarrow H_3O^+ + CO_3^{2-} \quad (17)$$

Reduction of corrosive species:

$$2HCO_3^- + 2e^- \leftrightarrow 2CO_3^{2-} + H_2 \quad (18)$$

$$2H_3O^+ + 2e^- \leftrightarrow H_2 + 2H_2O \quad (19)$$

$$2H_2O + 2e^- \leftrightarrow H_2 + 2OH^- \quad (20)$$

Dissolution of iron:

$$Fe \leftrightarrow Fe^{2+} + 2e \quad (21)$$

Formation of corrosion product:

$$Fe^{2+} + CO_3^{2-} \leftrightarrow FeCO_3 \quad (22)$$

where PZH^+, $PZCOO^-$, and H^+PZCOO^- are protonated-PZ, PZ carbamate, and protonated PZ carbamate, respectively.

3.1.3. EIS Analysis. In addition to LPR testing, the effect of exposure duration on the corrosion behavior of A106 in 0.43 C/N CO_2 loaded 30 wt % PZ has also been analyzed by EIS measurements. Figure 4 shows the obtained Nyquist plots of A106 after various exposure durations. The Nyquist plots depict a depressed semicircle or loop, the arc of which increased with increases in exposure time. This indicates that the corrosion rate may decrease with increases in time, which is consistent to the LPR results given in Figure 1. An equivalent circuit model was constructed to correlate the impedance behavior with capacitance and resistance. Based on the characterization results from SEM/EDS and XRD, this behavior can be explained by the model of a layer of corrosion product with defects,[11,35] and its equivalent electrical circuit is shown in Figure 5. R_s corresponds to the uncompensated resistance between the reference electrode and the test electrode, i.e., the resistance of solution or ohmic resistance. R_p is the pore resistance of the layer of $FeCO_3$. CPE_1 is the capacitance related to the layer of $FeCO_3$. R_{ct} is the charge transfer resistance, i.e., the resistance to the electron transfer of the faradic process at the carbon steel surface. CPE_2 is the capacitance related to the electric double layer. The parameters of the equivalent circuits are summarized in Table 2. The simulated data were also plotted in Figure 4. It can be seen that the fitting curves matched well with the experimental results. In addition, increases in R_{ct} and R_p were observed with increases in exposure duration (Table 2), which indicated that the corrosion resistance increased, i.e., a decrease in the corrosion rate as shown in Figure 1.

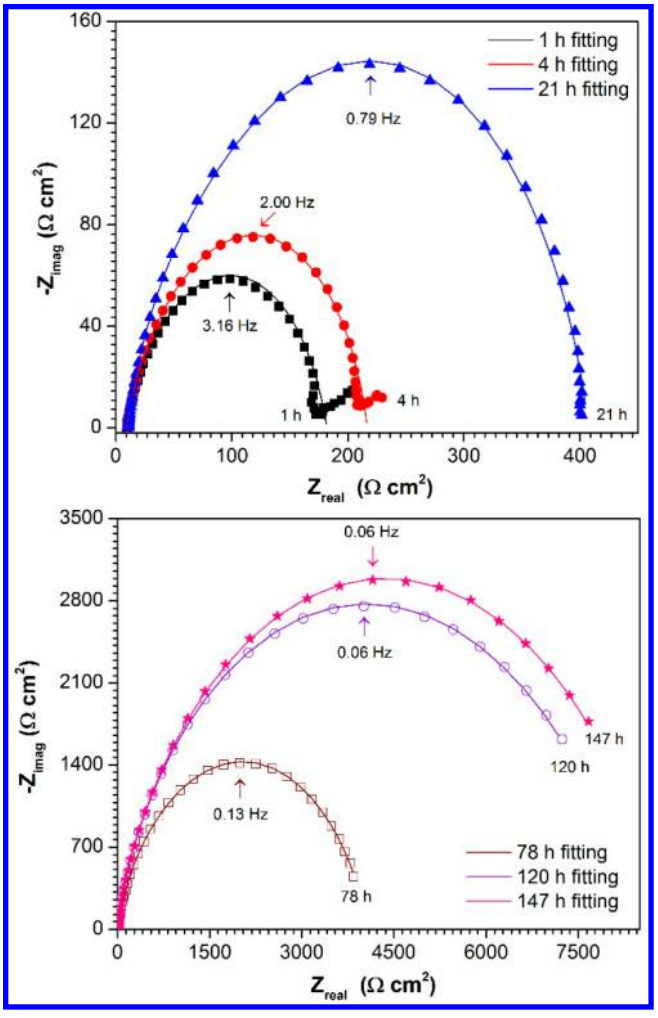

Figure 4. Nyquist plots of A106 in 0.43 C/N CO_2 loaded 30 wt % PZ solution at 80 °C to show duration effect, in which the black solid square is for 1 h, the red solid circle is for 4 h, the blue solid triangle is for 21 h, the orange open square is for 78 h, the purple open circle is for 120 h, and the pink solid star is for 147 h. Also, their fitting curves are shown by corresponding lines.

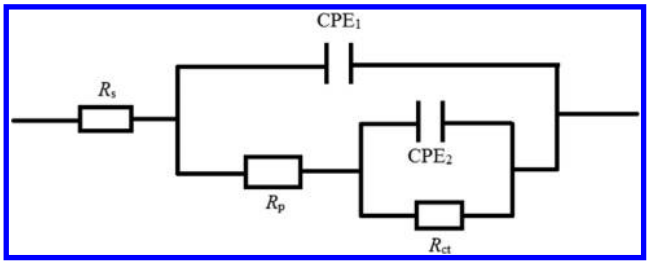

Figure 5. Equivalent electrical circuit used to analyze the EIS data recorded during corrosion of A106 carbon steel in 0.43 C/N CO_2 loaded 30 wt % PZ solution at 80 °C for different durations.

3.2. Long-Term Immersion Testing. To fully understand the corrosion behavior of A106 in CO_2-loaded 30 wt % PZ such as the effect of degradation products if any at the selected testing conditions, a long-term immersion corrosion test with more severe conditions (a CO_2 loading of 0.43 C/N, a temperature of 100 °C, and a pressure of 110 psi) that cannot be conducted with the electrochemical cell was performed in a traditional corrosion cell. The corrosion rates of A106 under various durations have been calculated from the weight loss method with eq 1. Figure 6 shows the calculated corrosion rates for different durations. The trend of the corrosion rate vs exposure duration is similar to that obtained from electrochemical testing at 80 °C (Figure 6), i.e., the corrosion rate decreased sharply from approximately 0.14 mmpy after 150 h to approximately 0.02 mmpy after 600 h. Thereafter, a steady-state corrosion process was observed with increases in duration up to 1050 h. From the XRD results shown in Figure 7, it indicates that the as-formed $FeCO_3$ was highly stable even after 1050 h immersion testing. Also, insignificant changes in the diffraction peaks for both $FeCO_3$ and Fe were observed with increases in duration from 150 up to 1050 h. This corroborates that the overall corrosion rate is low after 150 h, which is consistent to the results shown in Figure 1. However, the decrease in corrosion rate down to 0.03 mmpy is much faster in

dx.doi.org/10.1021/ie501346z | Ind. Eng. Chem. Res. 2014, 53, 11740−11746

Table 2. Summary of Parameters in an Equivalent Circuit Shown in Figure 5

duration (h)	R_s (Ω cm^2)	R_p (Ω cm^2)	CPE$_1$ (F/cm^2)	α_1	R_{ct} (Ω cm^2)	CPE$_2$ (F/cm^2)	α_2
1	9.47	129.41	4.85×10^{-3}	0.80	42.86	1.34×10^{-2}	0.83
4	10.05	149.04	3.86×10^{-3}	0.83	57.67	9.90×10^{-3}	0.90
21	10.62	248.22	1.87×10^{-3}	0.85	148.16	4.19×10^{-3}	0.84
78	10.78	1837.10	1.93×10^{-4}	0.88	2247.79	2.99×10^{-4}	0.65
120	11.36	2901.66	8.16×10^{-5}	0.89	5703.71	1.31×10^{-4}	0.56
147	11.44	3055.00	7.91×10^{-5}	0.89	5947.87	1.22×10^{-4}	0.61

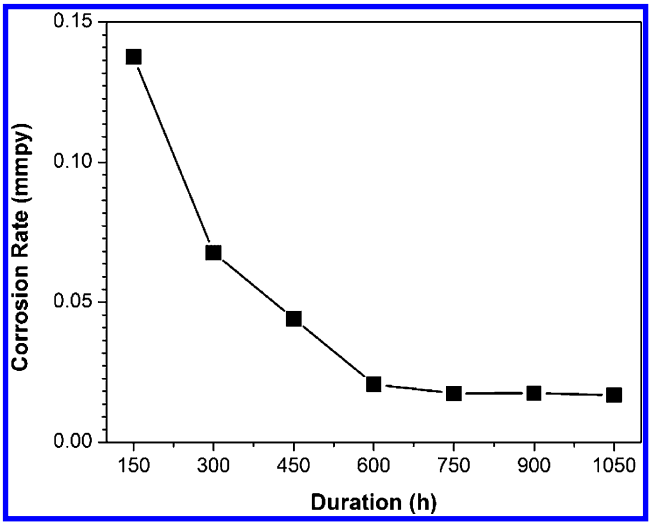

Figure 6. Corrosion rates of A106 carbon steel in ~0.43 C/N CO_2 loaded 30 wt % PZ at ~100 °C, obtained by weight loss method, as a function of immersion duration.

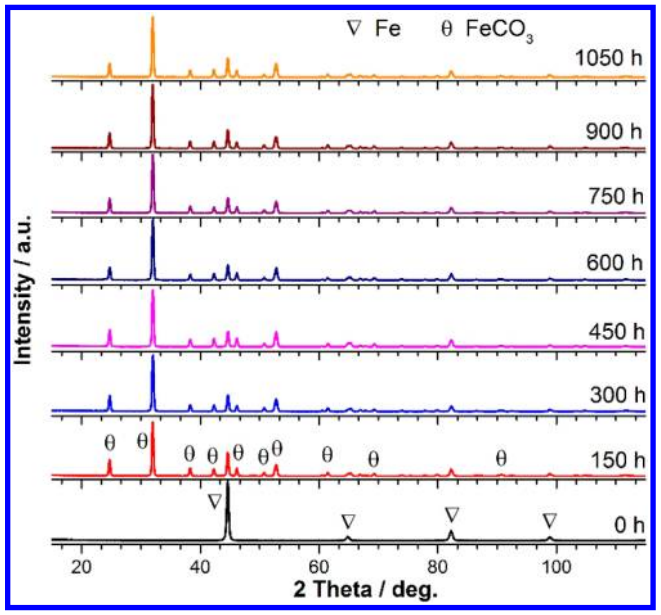

Figure 7. XRD patterns showed the stability of the formed layer of $FeCO_3$ on A106 in ~0.43 C/N CO_2 loaded 30 wt % PZ at ~100 °C up to 1050 h.

the short term electrochemical testing compared to that in long-term immersion corrosion testing. The difference is around 540 h. Two main reasons are responsible for this difference. The first one is the temperature is much higher for long-term immersion corrosion than that for short-term electrochemical testing, which would result in high kinetics for electrochemical reactions. The second one is that electrochemical testing was carried out under static conditions but long-term testing was carried out with circulation of the amine solution which would introduce erosion simultaneously.

Moreover, the as-formed $FeCO_3$ could not be removed physically by hand. This demonstrates that the layer is strong enough to withstand a certain degree of erosion resulting from fluid movement. Combined with all of the results from XRD and SEM/EDS under different exposure durations, the as-formed $FeCO_3$ was found to be highly dense and stable and could be an important reason for low corrosion in a 30 wt % PZ environment used for carbon capture. One of the other possible reasons for a low corrosion rate is the low degradation rate of PZ, especially in cases with low oxygen content such as the investigated conditions,[19−21] which led to fewer corrosive species such as ammonia and heat stable salts (HSS) that were reported to be an important factor in increasing the corrosion of steels in CO_2-loaded MEA.[15−17] Fe^{2+} content may also increase in PZ as oxidation products increase over time which may ultimately affect this protective layer. This effect will be investigated in future research.

4. SUMMARY

Corrosion of A106 carbon steel has been conducted in 0.43 C/N CO_2 loaded 30 wt % PZ and analyzed by electrochemical methods including LPR and EIS at 80 °C and long-term immersion testing (up to 1050 h) at 100 °C with a pressure of 110 psi. The as-corroded samples have been characterized by XRD and SEM/EDS. The results showed: (1) the formation of a dense, robust, stable, and protective $FeCO_3$ layer on the surface of A106 resulted in a sharp decrease of the corrosion rate followed by a steady-state corrosion process with low corrosion rate, (2) the benefits of the as-formed layer of $FeCO_3$ on carbon steel in PZ demonstrate that it may be a more attractive candidate as a carbon capture solvent, and (3) this coating could have a direct applicability toward lower corrosion rates in other amine CO_2 capture systems.

■ ASSOCIATED CONTENT

Supporting Information

Additional corrosion data, analysis for carbon-loaded piperazine, schematics for experimental setup, and comparisons to other amine systems. This material is available free of charge via the Internet at http://pubs.acs.org.

■ AUTHOR INFORMATION

Corresponding Author

*Tel.: +1 859 257 0293. Fax: +1 859 257 0220. E-mail address: kunlei.liu@uky.edu.

Notes

The authors declare no competing financial interest.

■ ACKNOWLEDGMENTS

The authors acknowledge the Carbon Management Research Group (CMRG) members, including Duke Energy, Electric Power Research Institute (EPRI), Kentucky Department of Energy Development and Independence (KY-DEDI), Kentucky Power (AEP), and LG&E and KU Energy, for their financial support. Also, the authors acknowledge suggestions and discussions from Ayokunle Omosebi, Xin Gao, and Naser Matin and solution analysis from Zhiao Li and Neal C. Koebcke.

■ REFERENCES

(1) Bert, M.; Ogunlade, D.; Hellen de, C.; Manuela, L.; Leo, M. *IPCC Special Report on Carbon Dioxide Capture and Storage*, first published ed.; Cambridge University Press: Cambridge, United Kingdom and NewYork, 2005; p 442.

(2) Rochelle, G. T. Amine Scrubbing for CO_2 Capture. *Science* **2009**, *325*, 1652−1654.

(3) Kohl, A.; Nielsen, R. *Gas Purification*, fifth ed.; Gulf Professional Publishing: Houston, TX, USA, 1997.

(4) DuPart, M. S.; Bacon, T. R.; Edwards, D. J. Understanding Corrosion in Alkanolamine Gas Treating Plants Part 1 & 2. *Hydrocarb. Process* **1993**, No. Apr/May, 3−11.

(5) Froning, H. R.; Jones, J. H. Corrosion of Mild Steel in Aqueous Monoethanolamine. *Ind. Eng. Chem. Res.* **1958**, *50*, 1737−1738.

(6) Bond, D. C.; Marsh, G. A. Corrosion of wet steel by hydrogen sulfide-air mixtures. *Corrosion* **1950**, *6*, 22−26.

(7) Gao, J.; Wang, S.; Sun, C.; Zhao, B.; Chen, C. Corrosion Behavior of Carbon Steel at Typical Positions of an Amine-Based CO_2 Capture Pilot Plant. *Ind. Eng. Chem. Res.* **2012**, *51*, 6714−6721.

(8) Soosaiprakasam, I. R.; Veawab, A. Corrosion and polarization behavior of carbon steel in MEA-based CO_2 capture process. *Int. J. Greenh. Gas. Con.* **2008**, *2*, 553−562.

(9) Kladkaew, N.; Idem, R.; Tontiwachwuthikul, P.; Saiwan, C. Corrosion Behavior of Carbon Steel in the Monoethanolamine−H_2O−CO_2−O_2−SO_2 System: Products, Reaction Pathways, and Kinetics. *Ind. Eng. Chem. Res.* **2009**, *48*, 10169−10179.

(10) Sun, Y.; Remias, J. E.; Neathery, J. K.; Liu, K. Electrochemical study of corrosion behavior of carbon steel A106 and stainless steel 304 in aqueous monoethanolamine. *Corros. Eng., Sci. Technol.* **2011**, *46*, 724−731.

(11) Sun, Y.; Remias, J. E.; Peng, X.; Dong, Z.; Neathery, J. K.; Liu, K. Corrosion behaviour of an aluminized nickel coating in a carbon dioxide capture process using aqueous monoethanolamine. *Corros. Sci.* **2011**, *53*, 3666−3671.

(12) Billingham, M. A.; Lee, C. H.; Smith, L.; Haines, M.; James, S. R.; Goh, B. K. W.; Dvorak, K.; Robinson, L.; Davis, C. J.; Peralta-Solorio, D. Corrosion and materials selection issues in carbon capture plants. *Energy Procedia* **2011**, *4*, 2020−2027.

(13) Pearson, P.; Hollenkamp, A. F.; Meuleman, E. Electrochemical investigation of corrosion in CO_2 capture plants—Influence of amines. *Electrochim. Acta* **2013**, *110*, 511−516.

(14) Veawab, A.; Aroonwilas, A. Identification of oxidizing agents in aqueous amine−CO_2 systems using a mechanistic corrosion model. *Corros. Sci.* **2002**, *44*, 967−987.

(15) Tanthapanichakoon, W.; Veawab, A.; McGarvey, B. Electrochemical Investigation on the Effect of Heat-stable Salts on Corrosion in CO_2 Capture Plants Using Aqueous Solution of MEA. *Ind. Eng. Chem. Res.* **2006**, *45*, 2586−2593.

(16) Rennie, S. Corrosion and materials selection for amine service. *Mater. Forum* **2006**, *30*, 126−130.

(17) Hofmeyer, B. G.; Scholten, H. G.; Lloyd, W. G. Contamination and Corrosion in Monoethanolamine Gas Treating Solutions. *Am. Chem. Soc., Div. Pet. Chem., Prepr.−Symp.* **1956**, *1*, 91−99.

(18) Aronu, U. E.; Hoff, K. A.; Svendsen, H. F. CO_2 capture solvent selection by combined absorption−desorption analysis. *Chem. Eng. Res. Des.* **2011**, *89*, 1197−1203.

(19) Freeman, S. A. Thermal degradation and oxidation of aqueous piperazine for carbon dioxide capture. Ph.D. thesis, The University of Texas at Austin, Austin, TX, 2011.

(20) Freeman, S. A.; Dugas, R.; Van Wagener, D. H.; Nguyen, T.; Rochelle, G. T. Carbon dioxide capture with concentrated, aqueous piperazine. *Int. J. Greenh. Gas. Con.* **2010**, *4*, 119−124.

(21) Freeman, S. A.; Davis, J.; Rochelle, G. T. Degradation of aqueous piperazine in carbon dioxide capture. *Int. J. Greenh. Gas. Con.* **2010**, *4*, 756−761.

(22) Bishnoi, S. Carbon Dioxide Absorption and Solution Equilibrium in Piperazine Activated Methyldiethanolamine. Ph.D. thesis, The University of Texas at Austin, Austin, TX, 2000.

(23) Dang, H. CO_2 Absorption Rate and Solubility in Monoethanolamine/Piperazine/Water. M.S. thesis, The University of Texas at Austin, Austin, TX, 2000.

(24) Cullinane, J. T. Thermodynamics and Kinetics of Aqueous Piperazine with Potassium Carbonate for Carbon Dioxide Absorption. Ph.D. thesis, The University of Texas at Austin, Austin, TX, 2005.

(25) Nainar, M.; Veawab, A. Corrosion in CO_2 Capture Process Using Blended Monoethanolamine and Piperazine. *Ind. Eng. Chem. Res.* **2009**, *48*, 9299−9306.

(26) ASTM Standard G4-95. *Standard Guide for Conduction Corrosion Coupon Tests in Field Applications*; ASTM: Philadelphia, PA, 2002.

(27) ASTM Standard G1-90 (Re-approved 1999), *Standard Practice for Preparing, Cleaning and Evaluating Corrosion Test Specimens*; ASTM: Philadelphia, PA, 1999.

(28) Duan, D.; Choi, Y. S.; Nesic, S.; Vitse, F.; Bedell, S. A.; Worley, C. Effect of Oxygen and Heat Stable Salts on the Corrosion of Carbon Steel in MDEA-Based CO_2 Capture Process. *Corrosion* **2010**, *10194*, 1−14.

(29) Mora-Mendoza, J. L.; Turgoose, S. Fe_3C influence on the corrosion rate of mild steel in aqueous CO_2 systems under turbulent flow conditions. *Corros. Sci.* **2002**, *44*, 1223−1246.

(30) Nešic, S.; Lee, K.-L. A mechanistic model for carbon dioxide corrosion of mild steel in the presence of protective iron carbonate films-Part 3: Film growth model. *Corrosion* **2003**, *59*, 616−628.

(31) Tanupabrungsun, T.; Young, D.; Brown, B.; Nesic, S. Construction and Verification of Pourbaix Diagrams for CO_2 Corrosion of Mild Steel Valid up to 250°C. *Corrosion* **2012**, *C2012-0001418*, 1−16.

(32) Xu, Q.; Rochelle, G. Total pressure and CO_2 solubility at high temperature in aqueous amines. *Energy Procedia* **2011**, *4*, 117−124.

(33) Dayalan, E.; Vani, G.; Shadley, J. R.; Shirazi, S. A.; Rybicki, E. F., Modeling CO_2 Corrosion of Carbon Steels in Pipe Flow. *Corrosion 1995*, NACE International: Houston, TX, 1995; paper no. 118.

(34) Heuer, J. K.; Stubbins, J. F. An XPS characterization of $FeCO_3$ films from CO_2 corrosion. *Corros. Sci.* **1999**, *41*, 1231−1243.

(35) Kendig, M.; Mansfeld, F.; Tsai, S. Determination of the long term corrosion behavior of coated steel with A.C. impedance measurements. *Corros. Sci.* **1983**, *23*, 317−329.